International Journal of Rock Mechanics & Mining Sciences 148 (2021) 104919

Contents lists available at ScienceDirect

International Journal of Rock Mechanics and Mining Sciences

journal homepage: www.elsevier.com/locate/ijrmms

# Expanding application of the voussoir beam analog to horizontally bedded and passively bolted flat-roof excavations using the discrete element method

Rami Abousleiman *, Sankhaneel Sinha, Gabriel Walton

*Colorado School of Mines, 1500 Illinois St Golden, CO, 80401, USA*

ARTICLE INFO

*Keywords:*
Numerical modeling
Discrete element method
Voussoir beam
Passive rock bolts

ABSTRACT

The voussoir beam analog is a well-established analytical method that has been successfully applied to the design of flat-roof excavations in discontinuous rockmasses. However, application of voussoir beam theory is limited to very specific conditions. Previous authors have attempted to account for more realistic loading and geometric conditions, but have not presented systematic or verified methods to account for variations in inelastic material behavior or supported roof geometry. This study presents multiple original numerical models that methodically assess the effects of increasing material and geometric complexity on voussoir beam mechanical behavior and develops adjustments to the Diederichs & Kaiser (1999) analytical solution to account for variations in post-peak material behavior and the interactions between multiple passively bolted layers. A step-by-step guide is presented for implementing these adjustments.

## 1. Introduction

Discontinuities are inherent features of bedded, jointed, and laminated rockmasses and can be significant controls on the mechanical response of excavations.[1] Depending on depositional environment, tectonic history, and current mining-induced stresses, the network of bedding planes, laminations, and fracture sets may violate many of the continuous, homogeneous, isotropic, and linearly elastic (CHILE) material assumptions that many practically applicable research and design methods rely on. Proliferation of computational power and discontinue numerical modeling methods allow geological engineers to simultaneously consider multiple, increasingly complex effects on excavation deformation that occur in-situ. However, the heterogeneous nature of many rockmasses can result in significant changes in ground conditions as a given excavation is advanced. These changes require additional models to understand the effects of multiple rockmass conditions on excavation response. Therefore, a practically applicable analytical method that can account for the mechanically relevant complexities remains desirable, regardless of advances in numerical methods.

Flat-roof excavations are commonly implemented in mining and civil-infrastructure projects in sub-horizontally to horizontally bedded sedimentary geologic formations. This excavation shape reduces excess material handling and prevents formation of fully unconfined rock blocks (i.e. blocks that are only bounded by the surrounding rockmass on two sides rather than three) while promoting formation of competent roof beams and enhancing roof self-supporting capacity. Flat-roof deformation mechanics have previously been studied predominantly via elastic and voussoir beam analogs.[2] Application of both elastic and voussoir beam theories to flat-roof excavations has specific limitations depending on the geologic and mining characteristics of a given design scenario. As this research is focused on laminated and discontinuous (i.e. cross-jointed) systems, the voussoir beam analog is more representative of the conditions considered herein. This research analyzes the voussoir beam mechanical response to more realistic intact rock behavior and the presence of passive support using the discrete element method (DEM) as implemented in Itasca's Universal Distinct Element Code (UDEC). The various voussoir beam model responses are then accounted for by identifying and adjusting relevant inputs to the existing Diederichs & Kaiser[3] analytical solution.

Even though DEM has been previously implemented in researching voussoir beam mechanics, studies often focus specifically on the influence of joint properties,[4] development of simplified analytical methods,[5] intact material properties and verification of analytical methods,[5,6] or individual case studies that range in rockmass complexity.[7–12] More

* Corresponding author.
*E-mail address:* rabousle@gmail.com (R. Abousleiman).

https://doi.org/10.1016/j.ijrmms.2021.104919
Received 4 March 2021; Received in revised form 19 August 2021; Accepted 10 September 2021
Available online 13 November 2021
1365-1609/

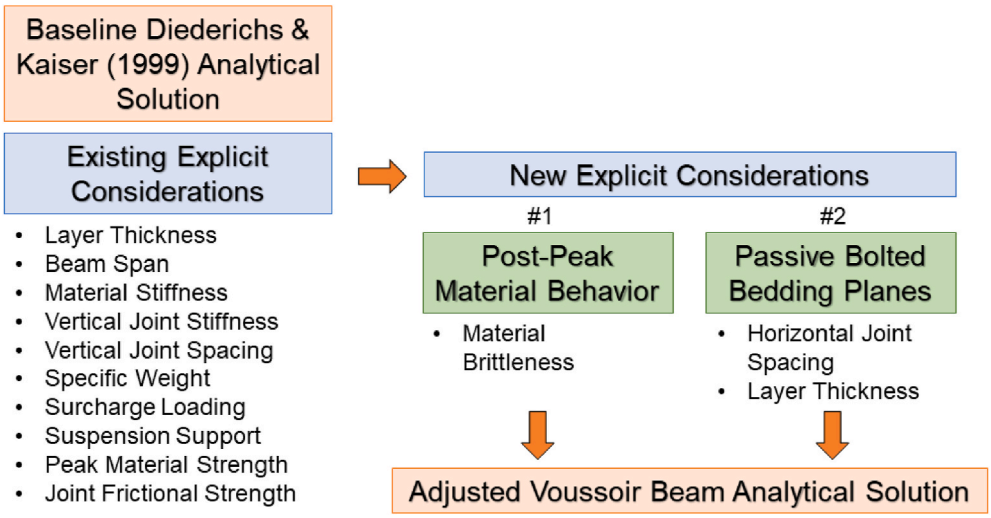


**Fig. 1.** Graphical depiction of exiting analytical inputs explicitly considered in the baseline Diederichs & Kaiser[3] analytical solution and the explicit considerations developed and validated through the course of this research.

recent studies have analyzed the impact of locked-in horizontal stress,[13,14] presence of active roof support,[15] and the transition from elastic beam behavior (i.e. massive, intact) to the development of tensile fractures and formation of a voussoir beam.[16] Notably, increasingly realistic material properties and roof geometries have not been thoroughly considered prior to application of the voussoir beam analog to more complex case studies.[3,11,12]

In order to expand the applicability of the voussoir beam analog to more realistic in-situ conditions, increasingly complex voussoir beam numerical models featuring inelastic intact material with various post-peak behaviors were analyzed, as were passively bolted multi-layer geometries. Existing modifications to the baseline Diederichs & Kaiser[3] voussoir beam analytical solution were considered, and adjustments identified and developed in the course of this study were found to be more accurate than the baseline Diederichs & Kaiser[3] analytical solution (Fig. 1). Ultimately, a guide on the limitations and implementation of the proposed modifications is presented to aid in future practical analyses.

### 1.1. Voussoir beam mechanical behavior

CHILE assumptions do not account for many observed in-situ rockmass characteristics and material properties such as: (1) fracture influence, (2) variation in rock strength and stiffness, (3) anisotropy, and (4) temporal effects of cyclical loading.[17] Removing the 'continuous' assumption and introducing vertical joints at the beam midspan and abutments brings the roof beam analog one step closer to capturing the in-situ mechanical behavior of excavation roof deformation in a discontinuous rockmass. This segmented beam geometry is known as a voussoir beam, first theorized by Evans[18] based on previous observations and experimentation by Fayol,[19] Jones & Llewellyn-Davies,[20] and Bucky & Taborelli.[21]

Generally, voussoir beam stability is governed by the span-to-thickness ratio (S/T) of the beam, and the strengths and stiffnesses of intact material and joints. Unlike simply supported elastic beams, voussoir beams carry zero or negligible tensile forces. The symmetric deflection of the bilateral beam spans through elastic shortening of the beam generates support via a horizontal thrust reaction force at discontinuities. The thrust transfers load to the abutments and supports the weight of the voussoir beam.[6]

The voussoir beam analog is traditionally applied in low-confinement scenarios where the immediate roof beam can be isolated from the complex loading conditions that sometimes occur in the field. Four main failure modes can occur in a voussoir beam geometry: (1) snap-through/buckling or elastic instability where the maximum possible resisting moment is surpassed by the overturning moment induced by the self-weight of the beam and any surcharge loads (no intact rock damage occurs); (2) crushing failure induced where maximum compressive stresses overcome the intact strength of rock at beam midspan and abutments; (3) vertical abutment slip prior to development of a sufficiently strong compressive arch or increasing surcharge load; and (4) diagonal tensile cracking normal to compressive forces.[3]

### 1.2. Analytical solutions

Despite the long history of voussoir beam research, analytical solutions for voussoir beam deflection, and maximum stresses are not as well-developed or constrained as simple elastic beams. This is reflected in the literature as variations in initial assumptions, boundary conditions, solution methods, and results. Methods such as iterative loop calculations, laboratory experiments, and numerical modeling have been employed in constraining expected and observed deformations and stresses in voussoir beams. Previous analytical solutions are available in Sterling,[22] Beer & Meek,[23] Sofianos,[24] and Diederichs & Kaiser.[3]

Diederichs & Kaiser[3] built upon Beer & Meek's[23] iterative solution loop and found that a stable voussoir beam in equilibrium will have a compression arch thickness of approximately 0.75 times the beam thickness (T) for small deflections and 0.3T at incipient collapse. Alejano et al.[11] indicated that the method in Diederichs & Kaiser[3] was more accurate at capturing in-situ conditions modeled than the analytical solution of Sofianos.[24] Mitra & Sofianos[25] have updated the original Sofianos[24] analytical solution to account for multi-jointed beams with stiff joints; however, this study is concerned with a wide range of joint stiffnesses when considering elastic intact material properties (as in Section 3). Therefore, the analytical solution from Diederichs & Kaiser[3] was used a baseline for comparison to the numerical models developed herein.

The spacing and normal stiffness of vertical joints were incorporated into a rockmass modulus ($E_{rm}$) by Diederichs & Kaiser[3]:

$$\frac{1}{E_{rm}} = \frac{1}{E} + \frac{1}{(jkn)s_j} \tag{1}$$

where jkn = joint normal stiffness, and $s_j$ = joint spacing. This adjustment is based on the equivalent stiffness of springs connected in series and assumes that the system is being loaded axially (i.e. perpendicular to

the joint orientation). The rockmass modulus for a single-layer beam calculated using Eqn. (1) based on only vertical joint spacing and stiffness is referred to as $E_{rmx}$ for the remainder of this paper.

Equations relating uniformly distributed surcharge and support pressures to the change in effective specific weight ($\gamma$) of the voussoir beam were also presented[3]:

$$\gamma^* = \gamma \pm \frac{q}{T} \tag{2}$$

where q = uniformly distributed pressure, and T = beam thickness. They suggested that using a triangular distribution can account for passive rock bolt elements providing suspension support and were able to consider the effect of cablebolts in a case study by using a negative pressure and decreasing the effective specific weight of the beam.

Following determination of the inputs depicted in Fig. 1, factors of safety (FoS) against buckling, crushing, and abutment slip (i.e. sliding) can be calculated with an iterative solution loop. Readers are referred to Diederichs & Kaiser[3] for a robust discussion of the iterative solution loop and effective specific weight.

Diederichs & Kaiser[3] also proposed a method of estimating rockmass modulus in-situ by using the Q tunneling index and the level of confinement of a given excavation. Furthermore, they suggested that in thinly laminated ground, grouted rebar should have a length equivalent to the desired beam thickness and that such beams should be designed to a FoS of 1.5–2.0. However, neither of these methods were fully validated, and accounting for support effect by adjusting the effective specific weight does not account for the doweling effect (i.e. shear resistance) of passive rockbolts, only the effect of suspension (i.e. axial resistance). Diederichs & Kaiser[3] evaluated their assessment of buckling failure using two case studies.

### 1.3. Consideration of complex geologic and mining conditions

Oliveira & Pells[14] evaluated orthogonally jointed and bolted 3-layer composite beam models that were 3.0 m thick; these models were analyzed considering various bedding plane properties, bolt orientations, and locked-in horizontal stresses. They noted that passive rockbolts installed on 1.75 m spacing, orthogonal to bedding did not promote composite beam behavior as much as passive bolts installed at a 70° angle to bedding. However, their results still showed an approximately 20% decrease in bolted beam displacement with bolts orthogonal to bedding. Beyond this study by Oliveira & Pells,[14] the explicit mechanical impact of passive bolts installed normal to the excavation roof has not been thoroughly explored in the context of the voussoir beam analog. In particular, the combined impacts of varying beam geometry and material properties.

Oliveira & Paramaguru[15] compared the impacts of complex loading and geometric conditions on voussoir beam numerical models to the analytical predictions of voussoir beam mechanics from Diederichs & Kaiser.[3] Oliveira & Paramaguru[15] presented an equation that provided a reasonable adjustment to the rockmass modulus used in the Diederichs & Kaiser[3] analytical solution based on the spacing of bedding partings. However, they only presented displacement results for a single bolted beam case that was supported with pre-tensioned bolts, leaving it inapplicable to passively bolted systems and its broader applicability uncertain given that only a single model case was considered.

It is evident that the body of research regarding roof stability in discontinuous sedimentary rock has confirmed that the voussoir beam analog can reasonably approximate roof deformation mechanics in flat-roof underground excavations. However, a connection between the simplified analogs presented above and the more complex loading conditions of laminated, discontinuous, and supported roofs has not yet been fully developed and verified in the literature.

## 2. Inelastic voussoir beams

Although elastic material assumptions may approximate in-situ conditions in competent, massive rockmasses, discontinuous and layered systems frequently include weak lithologies that deform inelastically. Sections 2.1-2.5 investigate the accuracy of assuming that voussoir beam collapse occurs coincidently with the onset of material yield through consideration of cases with various post-peak material behaviors. Three main causes contributing to differences between model results and the analytical solution were identified: midspan-abutment stress differential, analytical-model stress difference, and post-peak material behavior.

Note that only inelastic crushing failure was investigated in this section, while diagonal tensile cracking was not. This was due partly to the inability for the UDEC DEM implementation to explicitly model the rupture of intact material without the use of adaptations such as the bonded block method (BBM), and also because the inelastic beams modeled were not likely to incur diagonal tensile cracking failure due to their dimensions (i.e. S/T > 5) as indicated by physical models from Stimpson & Ahmed.[26] However, some model results indicated that a combination of crushing and diagonal tensile cracking failure might have occurred in some cases had explicit fracturing been allowed.

### 2.1. Methodology & model inputs

Multi-jointed inelastic voussoir beam models were created in UDEC based on those presented in Diederichs & Kaiser[3] with one exception: once voussoir arching was allowed to develop with effectively elastic joints (i.e. high cohesive strength, non-zero tensile strength), the joint constitutive model was changed to continuously yielding in order to capture the effect of realistic inelastic joint behavior on voussoir beam mechanics. The continuously yielding joint model has previously been shown to more accurately represent joint displacement under large deformation.[27] In addition to assuming zero tensile strength, it continuously relates the shear strength of the joint to the decay of friction from an initial (i.e. peak) to an intrinsic (i.e. residual) value, as well as a decrease in effective dilatancy as a function of plastic shear strain and normal stress acting on the discontinuity.

Voussoir beam abutments were modeled as elastic deformable blocks set to be functionally rigid (i.e. K = 5.6(10)[35] Pa). Diederichs & Kaiser[3] noted the use of rigid blocks in UDEC concentrated abutment stress and led to inaccuracies. This is due to the fact that rigid blocks are not discretized and only require an assigned density, therefore impacting stress calculations. Furthermore, the more recent versions of UDEC do not permit the use of fixed-velocity boundary conditions with rigid blocks, only deformable ones. The use of deformable abutment blocks with a high stiffness in the current UDEC models allowed for the impact of abutment block properties to be minimized and approach the assumptions and boundary conditions used in both the baseline Diederichs & Kaiser[3] analytical solution and the UDEC models featured therein.

The model solution method in Diederichs & Kaiser[3] was replicated by running models in multiple stages. The first stage featured strong intra-span and abutment joints with cohesion and tensile strength that allowed stable deflection to occur and horizontal stresses to develop in the voussoir beam. The second stage altered the intra-span joints to high-friction, zero cohesion, and zero tensile strength. The third stage altered the intra-span joints from Mohr-Coulomb to continuously yielding in order to model the impact of more realistic discontinuities once voussoir arching had developed. The fourth stage changed the intra-span joint parameters to realistic values, but left abutment joints with high frictional strength to maintain the assumption of zero abutment slip while allowing joint opening in accordance with the Diederichs & Kaiser[3] analytical solution and numerical models. Every time joint parameters were altered, the model was run to equilibrium. This method is discussed in detail and compared to the results of Diederichs & Kasier[3] in Abousleiman.[28]

**Table 1**
Geometric, discontinuity, Mohr-Coulomb parameters for intact material used in analyzing inelastic voussoir beam mechanical behavior. UCS* = in-situ intact compressive strength, E = Young's Modulus, v = Poisson's Ratio, $\Phi_i$ = initial friction angle, $\Phi_r$ = residual friction angle, $c_i$ = initial cohesion, $c_r$ = residual cohesion, $t_i$ = peak tensile strength, $t_r$ = residual tensile strength, $\psi$ = dilation angle, $\varepsilon_{cr}$ = critical plastic shear strain.

| Geometry & Discontinuities | | |
|---|---|---|
| **Beam Span (m)** | 10 | — |
| **Beam Thickness (m)** | 1 | – |
| **Joint Spacing (m)** | 0.5 | – |
| **Joint Stiffness (jkn/jks) (GPa)** | 100 | – |
| **Initial Joint Friction (°)** | 35 | – |
| **Intrinsic Joint Friction (°)** | 30 | – |
| **Intact Material Properties (Field-Scale)** | | |
| | **Strong** | **Weak** |
| **UCS* (MPa)** | 47 | 5.7 |
| **Density (kg/m$^3$)** | 2500 | 2500 |
| **E (GPa)** | 25 | 8 |
| **v** | 0.25 | 0.25 |
| **$\Phi_i$** | 40° | 20° |
| **$\Phi_r$** | 40° | 20° |
| **$c_i$ (MPa)** | 11 | 2 |
| **$c_r$ (MPa)** | $0.1c_i$ | $0.1c_i$ |
| **$t_i$ (MPa)** | 4 | 0.6 |
| **$t_r$ (MPa)** | $0.1t_i$ | $0.1t_i$ |
| **$\psi$** | 10° | 5° |
| **Strain Weakening $\varepsilon_{cr}$ (strain)** | $5.0(10)^{-3}$ | $5.0(10)^{-3}$ |
| **Brittle $\varepsilon_{cr}$ (strain)** | $1.0(10)^{-6}$ | $1.0(10)^{-6}$ |
| **Perfectly Plastic** | Residual=Peak | Residual=Peak |

All models in this section incorporated a block rounding of 0.015 m and a zone size of 0.2 m. The model setup, staging, block rounding, and zone size used were validated against the analytical solution and model results presented in Diederichs & Kasier.[3] For further information on baseline model validation, as well as zone size and block rounding sensitivity analysis, refer to Abousleiman et al.[29] and Chapter 2 of Abousleiman.[28]

Two rock-analogs representing reasonable end-member conditions were selected (referred to as weak and strong rock analogs, respectively), and the appropriate material properties were assigned based on Tulu et al..[30] Each rock analog was modeled with three post-peak behaviors: brittle, strain weakening, and perfectly plastic (Table 1). Both brittle and strain-weakening material were modeled with a residual strength equal to 10% of the peak strength, deviating from the common voussoir assumption that post-peak material strength is zero and that yield, failure, and beam collapse are coincident.

Although few weak (i.e. 5.7 MPa) geomaterials are likely to deform in an extremely brittle manner (e.g. coal), the unconfined nature of where material yield initiates (i.e. top of beam midspan and bottom of beam abutments) coupled with the need for direct comparison of end-member conditions led to the consideration of this case.

Both rock analogs listed in T were stable under self-loading in the voussoir geometry tested, so models were run with an increasing surcharge pressure (Fig. 2). Applied surcharge pressure increased the effective unit weight of the voussoir beam, increasing the maximum horizontal compressive stress generated, and decreasing the $FoS_{crushing}$.

Models were run by increasing the surcharge pressure in increments of 2.0 kPa, Eqn. (2) was used to recalculate a new effective specific weight, and the analytically predicted maximum stress was recalculated to identify the $FoS_{crushing}$ for each surcharge increment. After each increase in surcharge pressure, the model was solved to a standard equilibrium solution ratio of $1.0(10)^{-5}$ and stepped an additional 100,000 steps to ensure that the model had indeed stopped displacing.

Model histories of maximum horizontal stress at midspan and abutment, midspan deflection, and type of material yield were collected and compared to $FoS_{crushing}$ based on analytical predictions of displacement and horizontal stress.

$FoS_{crushing}$ was calculated in accordance with the method from Diederichs & Kaiser[3]:

$$FoS_{crushing} = \frac{UCS^*}{\sigma_{max}} \tag{3}$$

where $\sigma_{max}$ = maximum compressive stress determined by the voussoir analytical solution. The analytical solution assumes that when $FoS_{crushing} < 1.0$ (i.e. peak strength exceeded) the voussoir beam should immediately yield at the midspan and abutments, and collapse.

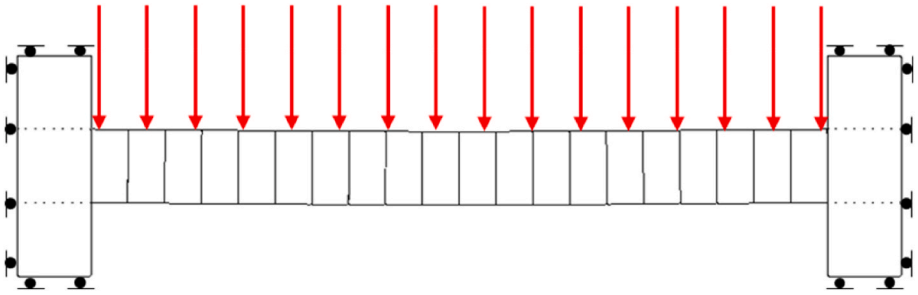

**Fig. 2.** Inelastic voussoir beam model geometry, surcharge load, and boundary conditions.

**Table 2**
Comparison of strain-weakening (SW), brittle, and perfectly plastic (PP) model results and analytically determined values of displacement and maximum stress at the surcharge where yield initiated. UCS* - in-situ compressive strength, kPa = kilopascal, cm = centimeter, MPa = megapascal, mid = midspan, abut = abutment, $\delta_{yy}$ = vertical displacement, $\sigma_{xx}$ = horizontal stress.

| | | Strong Rock Analog 47 MPa UCS* 310 kPa Surcharge | | | Weak Rock Analog 5.7 MPa UCS* 22 kPa Surcharge | | |
|---|---|---|---|---|---|---|---|
| | | **$\delta_{yy}$ (cm)** | **$\sigma_{xx,mid}$ (MPa)** | **$\sigma_{xx,abut}$ (MPa)** | **$\delta_{yy}$ (cm)** | **$\sigma_{xx,mid}$ (MPa)** | **$\sigma_{xx,abut}$ (MPa)** |
| **Analytical Solution (Diederichs & Kaiser[3])** | | 2.4 | 24 | 24 | 0.80 | 3.1 | 3.1 |
| **PP & SW** | **Model Result** | 2.5 | 28 | 45 | 0.67 | 3.3 | 6.1 |
| | **Analytical Error (%)** | −4.0 | −14 | −47 | 20 | −6.1 | −49 |
| **Brittle** | **Model Result** | 2.8 | 30 | 48 | 0.76 | 3.6 | 5.7 |
| | **Analytical Error (%)** | −14 | −20 | −50 | 5.3 | −14 | −46 |

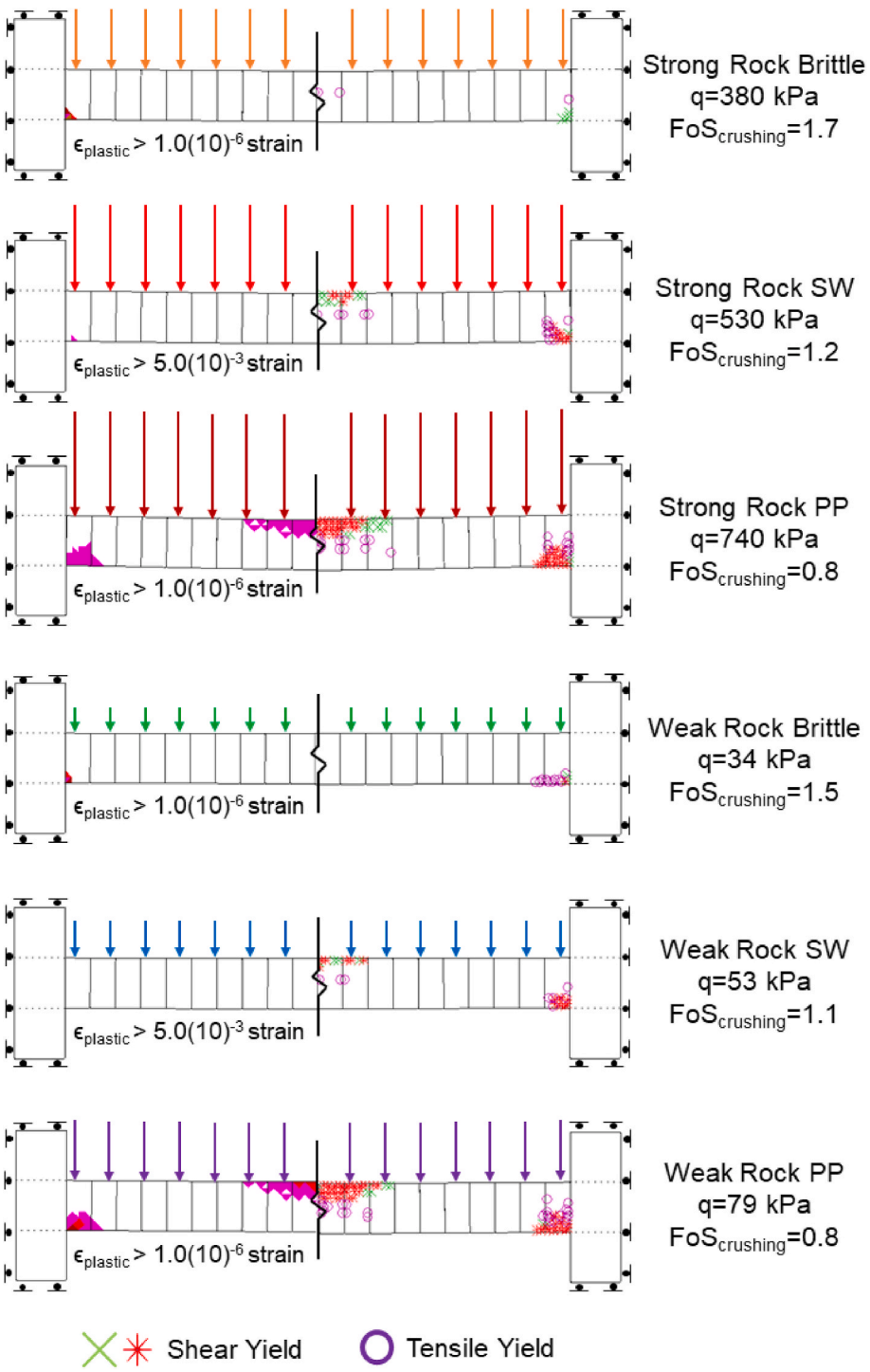


**Fig. 3.** Maximum stable surcharge pressure for simple inelastic voussoir beam model results showing yielded zone elements (right) and zones with plastic strains above the critical strain limit (left) at equilibrium for strong and weak beam models with brittle, strain-weakening, and perfectly plastic behavior. Surcharge pressure (q) and analytically determined $FoS_{crushing}$ shown. SW = strain-weakening, PP = perfectly plastic.

Diederichs & Kaiser[3] suggested multiplying the lab-scale UCS by 0.3–0.5 to account for scale effects and obtain a value for UCS*. However, as the properties listed in Table 1 are already field-scale values (i.e. UCS* rather than UCS), Eqn. (3) was compared to model results with no additional adjustment.

### 2.2. Initial yield results

Regardless of post-peak strength, material yield initiated at the beam abutments as the analytically determined $FoS_{crushing}$ approached 1.8 (i.e. 22 kPa surcharge pressure) and 2.0 (i.e. 310 kPa surcharge pressure) for the weak and strong rock analogs, respectively. Note that the voussoir beam analytical solution, which was used to calculate the $FoS_{crushing}$, tends to underpredict stresses at the beam abutments.[3] Therefore, the fact that yield initiated at approximately $FoS_{crushing} = 2.0$ has no direct relationship with the $FoS_{crushing}$ adjustment factors proposed (0.3–0.5 UCS) by previous authors[3,11] as those are based on material properties and scale, not differential stress concentrations (Table 2). The beam

**Table 3**
Comparison of strain-weakening (SW), brittle, and perfectly plastic (PP) model results and analytically determined values of displacement and maximum stress for the maximum stable surcharge for each material case tested. kPa = kilopascal, cm = centimeter, MPa = megapascal, mid = midspan, abut = abutment, $\delta_{yy}$ = vertical displacement, $\sigma_{xx}$ = horizontal stress.

| | | Strong Rock Analog 47 MPa UCS* | | | Weak Rock Analog 5.7 MPa UCS* | | |
|---|---|---|---|---|---|---|---|
| | | $\delta_{yy}$ (cm) | $\sigma_{xx,mid}$ (MPa) | $\sigma_{xx,abut}$ (MPa) | $\delta_{yy}$ (cm) | $\sigma_{xx,mid}$ (MPa) | $\sigma_{xx,abut}$ (MPa |
| **PP** | **Surcharge (kPa)** | | **740** | | | **79** | |
| | **Model Result** | 8.4 | 63 | 96 | 2.9 | 6.3 | 13 |
| | **Analytical Solution**[3] | 5.3 | 57 | 57 | 1.8 | 7.2 | 7.2 |
| | **Analytical Error (%)** | −37 | −9.5 | −41 | −38 | 14 | −45 |
| **SW** | **Surcharge (kPa)** | | **530** | | | **53** | |
| | **Model Result** | 5.1 | 48 | 90 | 1.4 | 5.8 | 10 |
| | **Analytical Solution**[3] | 3.9 | 40 | 40 | 1.3 | 5.3 | 5.3 |
| | **Analytical Error (%)** | −24 | −17 | −56 | −7.1 | −8.6 | −47 |
| **Brittle** | **Surcharge (kPa)** | | **380** | | | **34** | |
| | **Model Result** | 3.4 | 36 | 59 | 0.99 | 4.7 | 7.5 |
| | **Analytical Solution**[3] | 2.8 | 28 | 28 | 0.99 | 4.0 | 4.0 |
| | **Analytical Error (%)** | −18 | −22 | −53 | 0.0 | −15 | −47 |

geometry, block material density and Young's Modulus, joint stiffness, and joint spacing listed in Table 1 were implemented in the iterative solution loop in Diederichs & Kaiser[3] to calculate the maximum midspan displacement and beam horizontal stress.

At the onset of zone element yield, the voussoir analytical solution underpredicted maximum stresses for all model cases, particularly those stresses recorded at the beam abutments. This was due to a combination of the baseline analytical error (i.e. abutment-midspan discrepancy and surcharge error) and some yield-induced stress concentration. This discrepancy was generally consistent through all cases tested, but more pronounced in more brittle cases, as stresses were concentrated into fewer zones after yield. Results of perfectly plastic and strain-weakening models at yield initiation were effectively identical because the material had just entered the post-peak and the deviation in load bearing capacity was insignificant.

Error was also greater in stronger cases due to the increased surcharge pressure required to yield the stronger voussoir beam and the associated deviation from the analytical solution. This phenomenon is a product of the way that surcharge pressure is accounted for in the analytical solution by simply increasing the specific weight of the beam, rather than accounting for how the surcharge pressure is impacting shear displacement along vertical discontinuities and the resulting horizontal stress distribution across the beam.

In summary, the difference between model and analytical results at yield initiation was due to the midspan-abutment stress differential (assumed to be zero in the analytical solution), and the error associated with the simplifications made by the analytical solution regarding applied surcharge loading. It should be noted that the stress discrepancy between midspan and abutment was within the range reported in Diederichs & Kasier.[3]

Regardless of the discrepancy between midspan and abutment stresses, these results show that a beam capable of incurring inelastic deformation in beam block material does not immediately collapse following yield due to gradual post-yield deformation and the non-zero residual strength of the material modeled.

### 2.3. Incipient beam collapse results – post-peak material behavior

Following analysis of the models immediately after initial material yield, surcharge pressures were increased incrementally until the beams failed. As this research deviates from the conservative simplifying assumption that yield and beam collapse are coincident, surcharge pressures were augmented, and the associated beam responses are documented herein. Model results were expected to increasingly deviate from the Diederichs & Kaiser[3] analytical solution with increasing surcharge pressure and post-peak ductility, both of which contribute to increased inelastic strain within the beam block material following yield but prior to beam collapse.

The four brittle and strain-weakening voussoir beams tested failed at values of $FoS_{crushing}$ as predicted by the Diederichs & Kaiser[3] analytical solution that were greater than one, while the perfectly plastic beams failed at $FoS_{crushing}$ values less than 1.0. The maximum stable surcharge pressures tested and their associated impact on the distribution of plastic shear strain and zone yield in the brittle, strain-weakening, and perfectly plastic cases are shown in Fig. 3. Although the Diederichs & Kaiser[3] analytical solution assumes that crushing failure of the beam occurs as soon as yield initiates, in reality, some stable beam deflection may occur between the onset of yield and the point of beam collapse. Accordingly, the analytically predicted $FoS_{crushing}$ at failure will necessarily be less than or equal to the analytically predicted $FoS_{crushing}$ at which yield initiates (observed to be $FoS_{crushing}$ = 1.8–2.0 in Section 2.2). The degree to which $FoS_{crushing}$ at failure deviates from $FoS_{crushing}$ at yield depends on the post-peak behavior (i.e. combination of residual strength and critical plastic strain) of the intact rock material.

Analyzing the inelastic voussoir beam abutments under the maximum stable surcharge pressure allowed a clear description regarding the state of the beam immediately before collapse to be developed. The in-situ compressive strength of the intact rock has been exceeded, zone elements have yielded in shear and tension, and zone plastic strains have exceeded the critical plastic strain (i.e. zones are at residual strengths).

In the strain-weakening beam models, midspan zones incurred significant shear and tensile yield, but the beams remained stable because the plastic strain at the midspan had not exceeded the critical strain and zone material properties had not reached residual values. Similarly, brittle beam models remained stable with insignificant or no yield at the midspan, while zones at the abutment had already reached residual strength values. Once the surcharge increment was increased to the next step above what is shown in Fig. 3 (i.e. 2.0 kPa higher), the brittle and strain-weakening beam midspans exceeded the critical strain, reached residual strength values, and the beams failed. This confirmed that the midspan crushing was the critical control on crushing failure in brittle and strain-weakening models. This finding was further highlighted by beam models remaining stable when maximum model abutment stresses approached nearly twice the UCS* of the beam material (Table 3). These high stresses are due to the fact that as the post-peak behavior was altered from brittle to perfectly plastic, the adjacent yielded zones could provide more confinement to the zones carrying the maximum abutment stress (up to $\sigma_3$ = 11 MPa in the perfectly plastic strong rock case).

Irrespective of the analytical solution's conservativism (i.e. assumed coincidence of yield and collapse), or the variation in the analytically determined stress and displacement in comparison to inelastic beam

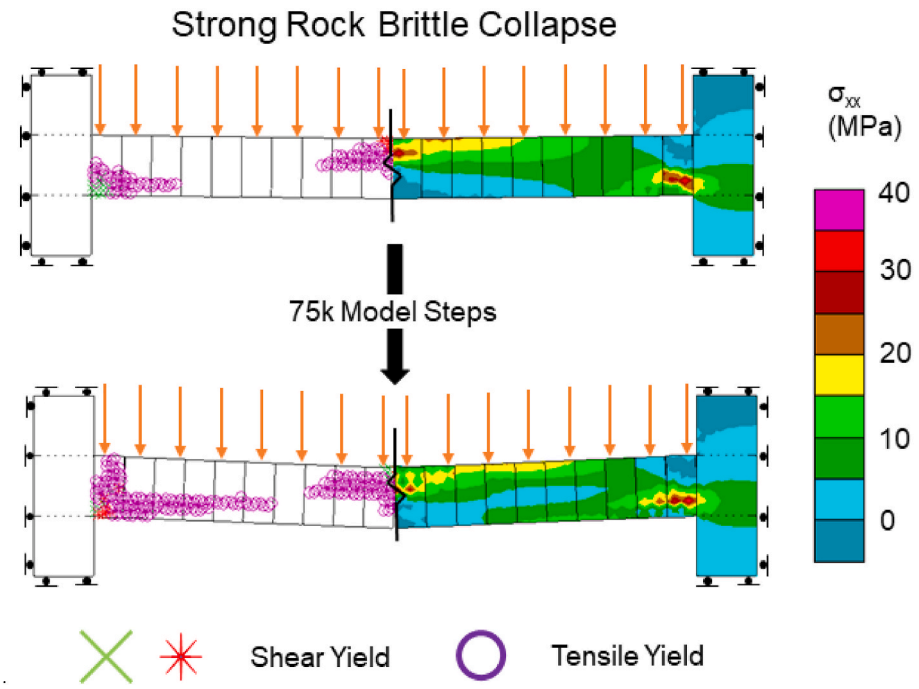


**Fig. 4.** Progressive collapse of strong rock brittle beam at ultimate surcharge pressure, initial midspan shear initiation (top left) and stress concentration away from the top of the beam (top right), progressive beam collapse and tensile damage showing yielded elements (bottom left) and compression arch deterioration (bottom right).

model results (i.e. optimistic), the analytically determined $FoS_{crushing}$ had no method to account for post-peak material behavior and therefore was both inaccurate and inconsistently conservative relative to the DEM model results considering post-peak behavior. However, the impact of midspan-abutment stress differentials, as well as the stress discrepancies between the analytical solution and model results countered that inconsistency with consistently optimistic stability predictions. Optimistic predictions (i.e. $FoS_{crushing} > 1.0$) occurred at both model yield initiation and collapse, particularly in the specific material cases (i.e. most brittle) that approach the analytical assumptions (i.e. beam collapse occurs at onset of material yield). Despite this consistency in determining displacement and stress, and consistent optimism when

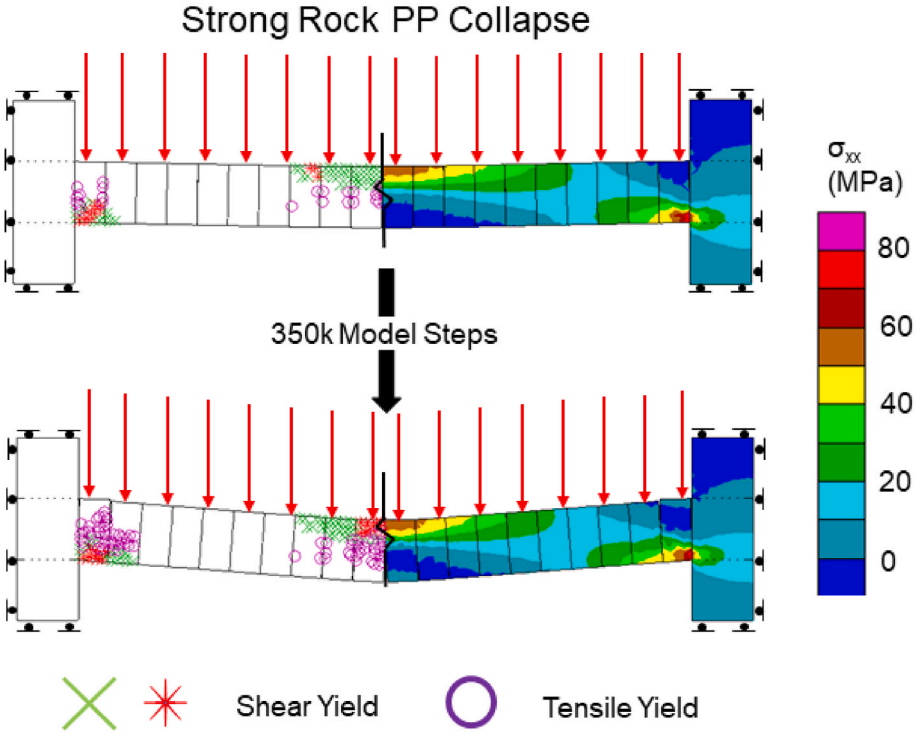


**Fig. 5.** Progressive collapse of strong rock perfectly plastic beam at ultimate surcharge pressure, initial yield status (top left) and horizontal arch (top right), progressive beam collapse and tensile damage showing yielded elements (bottom left) and maintained compression arch integrity (bottom right).

predicting crushing failure based on midspan-abutment and analytical-model stress differentials, $FoS_{crushing}$ is still clearly dependent on post-peak material behavior as beams modeled with field-scale strength properties failed at three different values of analytically calculated $FoS_{crushing}$.

Although the strain-weakening and brittle beams collapsed at analytically determined $FoS_{crushing} > 1.0$ (i.e. optimistic analytical solution prediction of stability), consideration of realistic post-peak material properties can only increase the stability of a given beam as the analytical solution assumes that yield and collapse occur simultaneously. Therefore, the overly optimistic analytical solution in brittle and strain-weakening beams is based partially on the underprediction of maximum midspan stress at the maximum stable surcharge load (9–22%). If the analytical solution matched the modeled beam midspan stresses at ultimate load, the strain-weakening beams would fail at exactly $FoS_{crushing} = 1.0$, but the strong and weak brittle beams would fail at 1.3 and 1.2, respectively. To account for this remaining discrepancy, the collapse mechanics of the modeled beams must be considered, namely the influence of tensile yield.

### 2.4. Final beam collapse results – tensile influence

Following analysis of the models immediately prior to beam collapse, surcharge pressures were increased an additional step (i.e. 2.0 kPa) and the beams failed. Each post-peak behavior case described above followed a distinct pattern of yield and collapse. In brittle beams, additional tensile yield occurred adjacent to zones that previously yielded in tension near the midspan and abutment. Shortly thereafter, the midspan yielded in shear and the voussoir compression arch immediately began to break down. Compression arch deterioration occurred in tandem with tensile yield propagation between the midspan and abutment, until total collapse of the beam occurred (Fig. 4).

The initial tensile yield at the midspan shown in Fig. 3 occurred in the zones at the periphery of the compression arch. The resultant failure shown in Fig. 4 appears to be tensile-yield-induced stress concentration causing midspan crushing, followed by a concurrent diagonal tensile cracking due to the brittleness of the material, independent of its peak strength, as the weak rock brittle beam failed in a similar manner. However, abutment and midspan crushing clearly preceded the tensile yield propagation between the two, whereas diagonal tensile cracking failure has been noted to occur without associated crushing of the midspan or abutments.[26]

When considering the strain-weakening beam collapse, a similar amount of shear yield and the pattern of compression arch deterioration occurred, but the beam failed without tensile yield propagating fully from midspan to abutment and the shear failure of the midspan was not preceded by stress concentration due to tensile yield surrounding the midspan.

Conversely, perfectly plastic beams failed at analytically determined FoScrushing $< 1.0$ (i.e. conservative analytical solution prediction of stability). The failure of the perfectly plastic beams occurs because both elastic and plastic strains contribute to the deflection and eventual overcoming of a relatively constant maximum horizontal stress (i.e. moment arm), rather than a sudden loss of strength and compression arch deterioration. This is clearly captured by the continuous and sustained horizontal compression arch as the moment arm decayed until ultimate collapse without associated tensile yield bridging between the abutment and midspan (Fig. 5).

### 2.5. Inelastic beam discussion

While the analysis above did not cover every possible rock type, perfectly plastic material behavior corresponded to an upper-bound estimate of post-peak strength, and brittle material behavior represented the lower-bound. These results indicate that application of $FoS_{crushing}$ to rocks and rockmasses with various post-peak material behaviors could significantly overestimate (i.e. failure occurs at $FoS_{crushing} > 1.0$) or underestimate (i.e. failure occurs at $FoS_{crushing} < 1.0$) the safety of a given roof span. This was due to a combination of differences in analytically determined maximum stress and model stress results, post-peak behavior of the material modeled, and model tensile yield.

The baseline Diederichs & Kaiser[3] analytical method, which already applies a correction factor of 0.3–0.5 to get from lab to field scale UCS, requires an additional adjustment based on the post-peak behavior of the rock. The current results suggest that an additional adjustment on the order of 0.6- or 1.25-times be made to Eqn. (3) for brittle and perfectly plastic rock types, respectively, once the UCS has been adjusted to field scale values and the post-peak material behavior is consistent and well-known. This adjustment should be applied with caution, however, until additional research verifies these findings.

**Table 4**
Proposed material and geometric properties for parametric analysis to verify adjustment to rockmass modulus in the existing voussoir beam analytical solution. Note that highlighted rows were varied concurrently and that remaining relevant bolt properties are from Bahrani & Hadjigeorgiou.[31]

| | | | |
|---|---|---|---|
| **Beam Span (m)** | 10 | 20 | --- |
| **Beam Thickness (m)** | 1 | 2 | 4 |
| **Horizontal Joint Spacing (m)** | 0.5 | 1 | --- |
| **Vertical Joint Spacing (m)** | 0.5 | 1 | 2.0 |
| **Bolt Spacing (m)** | 1.2 | 1.8 | 2.4 |
| **Bolt Element Node Spacing** | 24/m | --- | --- |
| **Bolt Normal Stiffness ($N/m^2$)** | $5.0(10)^{10}$ | --- | --- |
| **Bolt Shear Stiffness ($N/m^2$)** | $2.5(10)^{7}$ | --- | --- |
| **Bolt Normal Cohesion (N/m)** | $4.0(10)^{6}$ | --- | --- |
| **Bolt Shear Cohesion (N/m)** | $6.0(10)^{5}$ | --- | --- |
| **Joint Stiffness (jkn/jks) (GPa/m)** | 5.0 | 50.0 | 100.0 |
| **Intact Young's Modulus (GPa)** | 10.0 | 50.0 | 100.0 |

## 3. Orthogonally jointed & bolted beams

Following analysis of the impact of inelastic block post-peak material behavior, the impacts of horizontally jointed and supported roof conditions were considered through the use of elastic block models in this section. Although the joint networks, bedding planes, and supported roof conditions analyzed in this section correspond to more complex multi-beam geometries than have been previously considered, they represent the simplest possible case with fully persistent and evenly spaced horizontal and vertical discontinuities.

### 3.1. Methodology & model inputs

First, the effect of passive bolts was considered on a limited suite of models transitioning from a single-layer, 1 m thick beam, to a two-layer, 1 m thick beam (i.e. two 0.5 m layers), and finally to a single-layer 0.5 m thick beam. The results of this preliminary effort identified a trend in the overall beam behavior that warranted an expanded investigation. Furthermore, the degree by which the bolt element and interface were loaded by the deflecting layers were identified.

In order to approach in-situ roof geometry of a discontinuous and layered rockmass, a suite of voussoir beam models with multiple voussoir layers tied together using passive rockbolt elements encompassing the properties in Table 4 were developed. All combinations of properties were tested resulting in 810 original numerical models. Models were run using the previously described method transitioning from elastic joints to continuously yielding, as well as a block rounding value of 0.015 m and zone size of 0.125 m previously validated by comparison to the baseline Diederichs & Kaiser[3] analytical solution in Abousleiman et al.[29] and in Chapter 2 of Abousleiman.[28]

The modeled rockbolt structural elements provide axial and shear

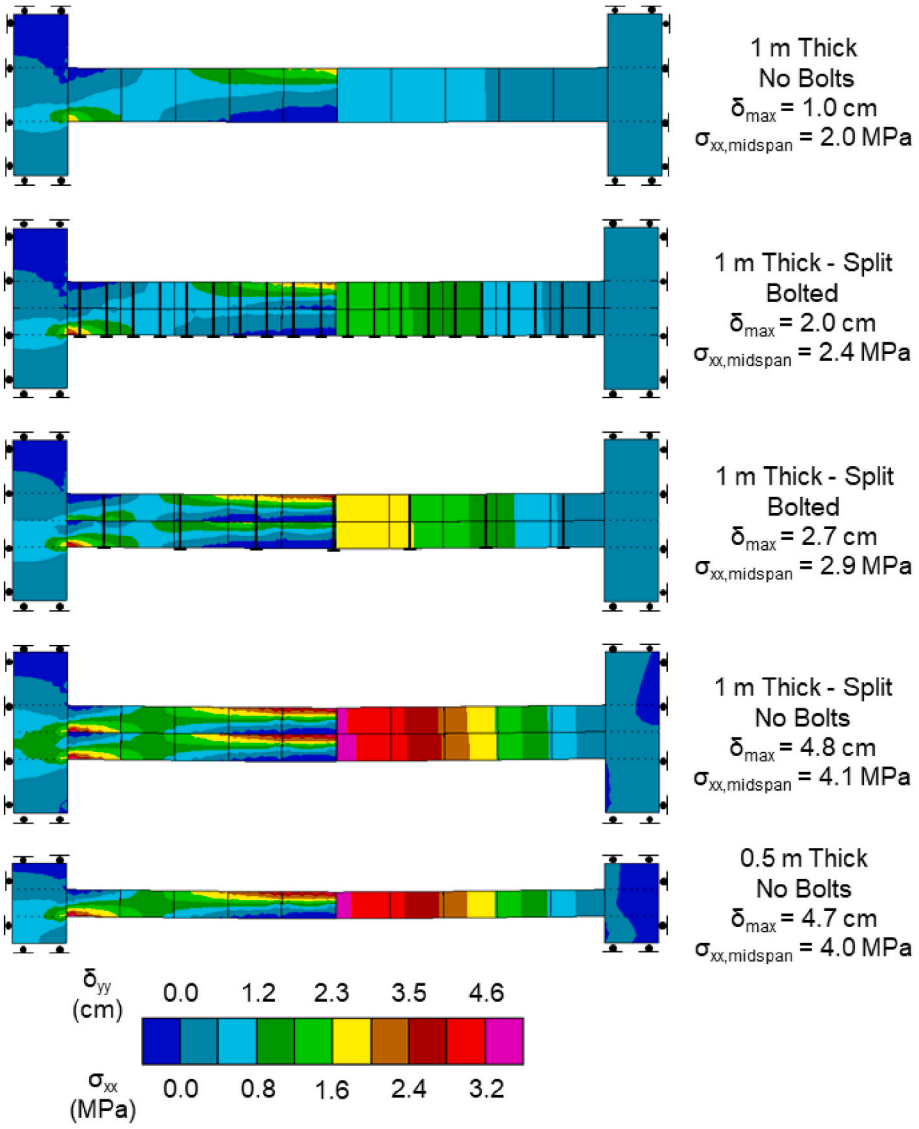


**Fig. 6.** Comparison of horizontal stress (left) and vertical displacement (right) results of multiple beam geometries ranging from a single, unbolted, 1 m thick beam (top) to a single, unbolted, 0.5 m thick beam (bottom), and variations in between featuring different bolt spacings and properties. All beams have an $E_{rmx} = 3.3$ GPa.

resistance based on the parameters developed by Bahrani & Hadjigeorgiou[31] through calibration of UDEC models to laboratory testing of pure axial and shear loading of fully-grouted rebar rockbolts. The rockbolt element constitutive model in UDEC treats the rock-grout-bolt system as a linearly elastic material up to an ultimate tensile failure (rupture) strain, and uses spring-slider elements to model interaction between the bolt and the surrounding material. The strength of the interface between the bolt and the surrounding material depends on the slider element cohesion and friction, while the stiffness values control the elastic response of the spring.[32]

Model results were considered in relationship to the baseline Diederichs & Kaiser[3] analytical solution with varying degrees of accuracy, generally decreasing with increased maximum model displacement. A method of accounting for the effect of multi-layered bolting of a discontinuous rockmass into a single Young's Modulus for use in the baseline Diederichs & Kaiser[3] analytical solution could not be identified in the literature. Generalized application of anisotropic rockmass deformation moduli require knowing the unique states of stress (i.e. vertical, horizontal, and shear) and relating them to strains using a deformation modulus matrix,[33–36] rather than calculating an unknown maximum state of stress from elastic strains and a uniform stiffness.

A statistical analysis of the stable model results was performed in an effort to identify potential modifications to the analytical solution. A method of resolving the anisotropic stiffness of a multi-layered bolted beam into a single effective Young's Modulus based on the number of bolted layers was developed. This was done by using the *fminsearch* function in MATLAB to determine the rockmass modulus that minimized the difference between model displacement results and analytical predictions of maximum displacement for each case. As previously stated, the rockmass modulus calculated by consideration of only vertical joints in Eqn. (1) is referred to as $E_{rmx}$. The rockmass modulus back calculated by using the *fminsearch* function is referred to as the effective or the minimized $E_{rm}$. The rockmass modulus determined as a result of the statistical analysis of model inputs and the effective $E_{rm}$, is referred to as the layer-adjusted $E_{rm}$ ($E_{rmn}$).

Multiple linear regressions were fit to the data set based on the minimized $E_{rm}$ (i.e. dependent variable), and its relationship with $E_{rmx}$, and the number of horizontal layers (i.e. independent variables). A trend was identified and $E_{rmx}$ was adjusted to predict the displacement of multi-layered voussoir beams. This method was then verified by determining how well the analytical solution incorporating the layer-adjusted $E_{rm}$ and bolted interval thickness, could predict binary stability (i.e.

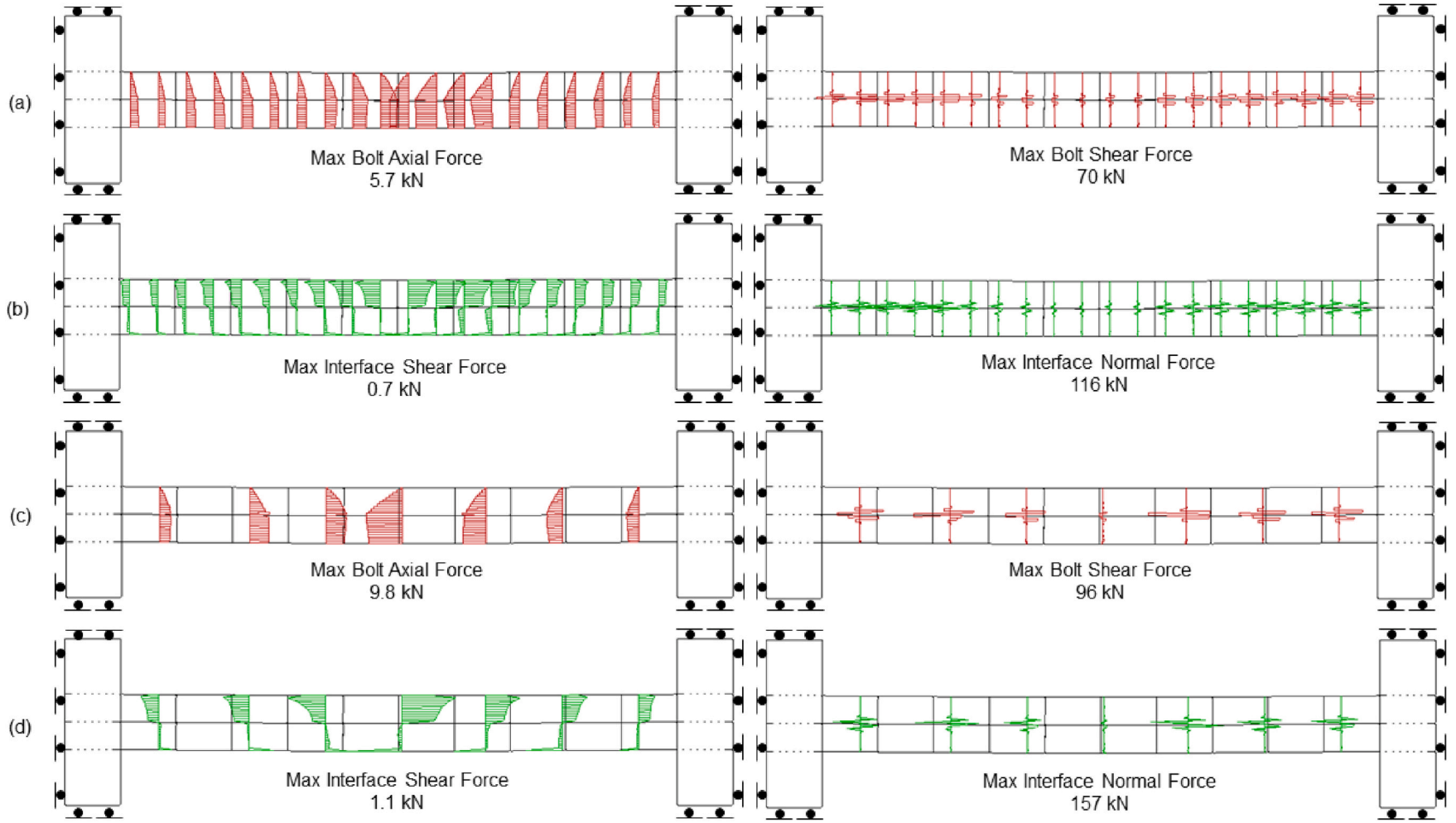


**Fig. 7.** Rockbolt (a,c) element and (b,d) interface axial, shear, and normal force plots for two preliminary bolted models with (a,b) 0.5 m and (c,d) 1.4 m bolt spacing.

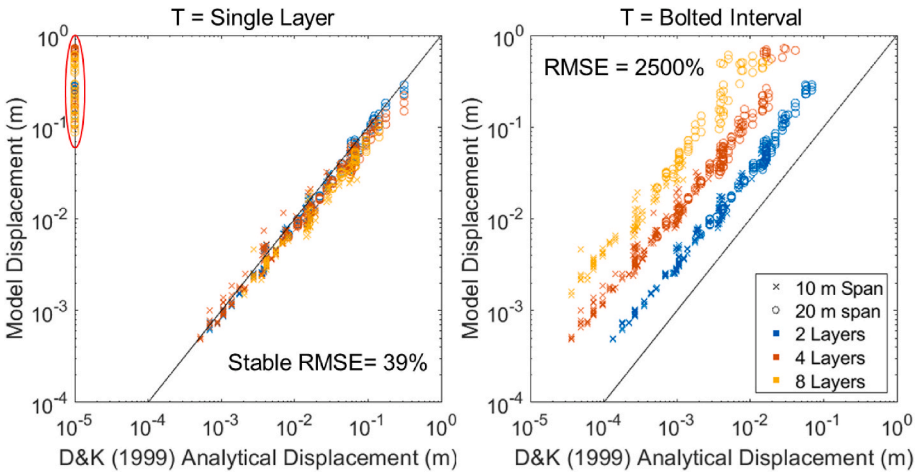


**Fig. 8.** Comparison of the predicted displacement by the Diederichs & Kaiser[3] analytical solution and model displacement results when considering the thickness input to be a single layer (left), or the entire bolted beam interval (right). Note that results that plot on the y-axis (i.e. x = $1.0(10)^{-5}$, circled in red) indicate that the analytical solution predicted an unstable result, but model results indicated stability had been maintained. A 1:1 trend line is shown in black and the percent root mean square error for results where both the model and the analytical solution predicted stability is shown; note the log-log axes. (For interpretation of the references to colour in this figure legend, the reader is referred to the Web version of this article.)

stable or unstable) and maximum displacement of multi-layered bolted voussoir beam models in comparison to the baseline Diederichs & Kaiser[3] method.

However, the layer-adjusted $E_{rm}$ method remained inaccurate for predicting horizontal stresses due to its significant reduction in rockmass modulus and increase in beam thickness. A similar statistical analysis was therefore utilized to back calculate an optimized effective thickness between the individual layer and bolted interval thickness for the purposes of estimating beam stresses.

### 3.2. Influence of passive bolts

Comparison of beam displacement and horizontal stress distribution for the preliminary suite of beam geometries indicated that the bolted beam response (i.e. displacement and stress) was bounded by the responses of the two single-layer beams and was impacted by the degree of passive bolting (Fig. 6).

Comparison of bolt shear and axial load response in the two bolted models indicated that support was being activated in the passive bolts even under relatively stable conditions (Fig. 7). The bolts closer to the midspan were taking on higher axial loads, while the bolts closer to the abutments were taking on higher shear loads. Overall, the shear loads were an order of magnitude higher than the axial loads, indicating that although some suspension of the lower layer had occurred, the primary support mechanism was the generation of shear resistance along the horizontal discontinuity between layers. In particular, the dowelling effect of rockbolts raised the apparent cohesion of the discontinuity, while preventing the separation of the two beams increased the discontinuity's frictional strength.[2] Because the relative shearing between the two beams was prevented, the system effectively behaved similarly to a single beam.

The observed joint behavior in the models was consistent with the degree of axial and shear loading of the bolt elements and interfaces. Models with fewer bolts incurred higher shear displacements along bedding planes closer to the abutments, increasing the bolt element shear force and interface normal force. Conversely, shear displacements along vertical joints remained consistent throughout all the models presented in this section. Models with fewer bolts also incurred higher bedding plane separation at the beam midspan, increasing the bolt element axial force and interface shear force.

Vertical joint separation at the top of the abutments and bottom of the midspan was proportional to the beam displacement (i.e. effective overall stiffness of the beam). Recall that as a beam deflects the top contracts, and the bottom expands. This incurs shearing along the horizontal joint, which is limited by the bolts in the supported models. Increasing the number of bolts reduces the shear, increasing the effective thickness and stiffness of the orthogonally jointed and supported beam. Per classical beam theory, deflection is inversely proportion to flexural rigidity, and rigidity is proportional to thickness cubed and the elastic modulus of the beam.

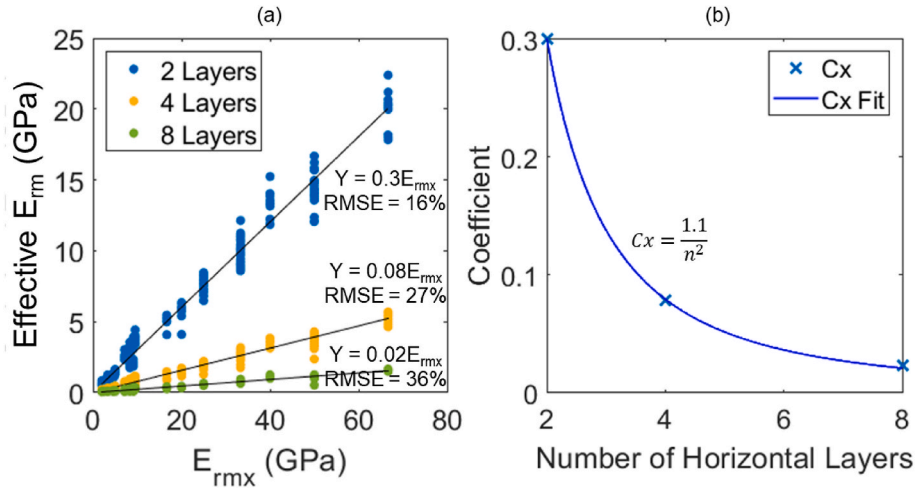


**Fig. 9.** Statistical analysis fitting the effective $E_{rm}$ to $E_{rmx}$ (a) and the resulting impact on the relationship between the coefficient of $E_{rmx}$ (Cx) and number of horizontal layers (b). Note that $R^2$-adjusted values for 2, 4, and 8-layer regressions are 0.98, 0.97, and 0.95 respectively.

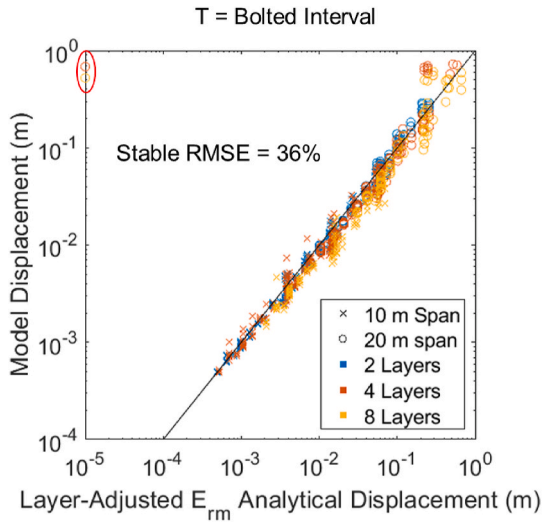


**Fig. 10.** Comparison of the predicted displacement by the layer-adjusted $E_{rm}$ analytical method and stable bolted model displacement results. The layer-adjusted $E_{rm}$ is used in conjunction with the thickness of the bolted interval. The results that plot on the y-axis (i.e. x = $1.0(10)^{-5}$, circled in red) indicate that the analytical solution predicted an unstable result, but model results indicated stability had been maintained. A 1:1 trend line is shown in black and the percent root mean square error for results where both the model and the adjusted analytical solution predicted stability is shown; note the log-log axes. (For interpretation of the references to colour in this figure legend, the reader is referred to the Web version of this article.)

### 3.3. Beam stiffness-displacement analysis results

The Diederichs & Kaiser[3] analytical solution was tested against stable model displacement results considering both the entire beam thickness (as suggested by Diederichs & Kaiser[3]), as well as the individual layer thickness, with varying degrees of accuracy (Fig. 8).

In stable model results, the accuracy of the baseline solution was not significantly impacted by increasing beam displacement when using the individual layer thickness. However, misclassification of 69 stable cases as unstable and a general increase in overprediction of displacement with increasing model displacement is shown in Fig. 8. If the misclassified models were not considered, this method maintained reasonable accuracy for predicting displacement with an RMSE of 39%. This result indicates that for highly self-stable beams, the displacements are smaller, passive bolt support is not activated to the same degree, and the independent voussoir beams corresponding to each layer deflect more or less uniformly. When using the bolted interval thickness (as suggested in Diederichs & Kaiser[3]), displacement is consistently and significantly underpredicted by the Diederichs & Kaiser[3] analytical solution. However, distinct trends based on the number of passively bolted horizontal layers emerged from the dataset. In a practical scenario, if these trends could be described in terms of geomechanical parameters known prior to construction, the decrease in effective stiffness noted in the transitional beam models of this study and by others (Pells & Best[12]; Oliveira & Pells[14]) could be predicted; this would allow for the behavior of such beams to be studied using the existing analytical solution without the need for numerical modeling.

Using the *fminsearch* function in MATLAB, an effective $E_{rm}$ was back calculated by minimizing the difference between model and analytical displacement for T = bolted interval. The effective $E_{rm}$ was then compared to the $E_{rmx}$ and number of bolted layers to develop the $E_{rmn}$ equation for practical application (Fig. 9).

Based on the statistical analysis above, the following equation was developed:

$$E_{rmn} = (Cx)E_{rmx} \quad (4)$$

Note that in a single layer case, Cx is equal to 1.1 and Eqn. (4) is nearly equal to Eqn. (1).

The $E_{rmn}$ was then substituted for $E_{rmx}$ in the Diederichs & Kaiser[3] analytical solution and compared to model results of maximum displacement (Fig. 10).

Using $E_{rmn}$ in the Diederichs & Kaiser[3] analytical method allowed for consideration of the bolted interval thickness, reduced RMSE to 36% when compared to the baseline method, and accurately classified the stability of 67 formerly misclassified stable models, leaving only two misclassified model results in total. These results verified that the $E_{rmn}$ method more accurately captured orthogonally jointed and bolted beam displacement than the baseline Diederichs & Kaiser[3] analytical solution. However, some variance in the layer-adjusted method remains unaccounted for by this simplified approach (see Fig. 9a). To that end, multiple linear regressions considering various combinations of other model inputs (e.g. bolt spacing, explicit vertical joint spacing, etc.) were undertaken.

Although some of the individual and combined additional model inputs had statistically significant (i.e. p-value $< 0.05$) coefficients, they had no meaningful impact on the $R^2$-adjusted value of the original two-dimensional regression presented in Fig. 9a. This indicates that the regression presented sufficiently accounts for the statistically relevant complexities of the model cases tested in this study.

### 3.4. Beam thickness-stress analysis results

As in the case of the approach developed in the previous section, developing an approach to predict stresses in passively bolted beams through the identification of an appropriate effective stiffness for use in a well-vetted analytical solution has the potential to expand the practical applicability of the solution to more realistic geologic and mining conditions. The baseline Diederichs & Kaiser[3] analytical solution was tested against stable model midspan and abutment stress results considering both the entire beam thickness (as suggested by Diederichs & Kaiser[3]), as well as the individual layer thickness, with varying degrees of accuracy (Fig. 11).

Note that the same 69 stable models were classified as unstable by the analytical solution when considering T = single layer thickness. If the misclassified models were not considered, the baseline method maintained reasonable accuracy for predicting model stresses, with RMSE values of 48% and 29% for midspan and abutment stresses, respectively. When using the bolted interval thickness, both midspan and abutment stresses are consistently and significantly underpredicted by the baseline Diederichs & Kaiser3 analytical solution. In considering both analyses (single layer vs. bolted thickness), it appears that the trends in maximum horizontal stress can be related to some interaction between individual layer thickness and bolted thickness as governed by the properties of the beam material, discontinuities, and bolt elements.

Another optimization using *fminsearch* in MATLAB was used to identify the effective beam thickness in the analytical solution that best predicted the maximum midspan stress in a multi-layered bolted beam. However, this was complicated by the difference in midspan and abutment stress (i.e. which should be considered?) and the consideration of rockmass modulus (i.e. should $E_{rmn}$ or $E_{rmx}$ be used in back calculating an effective beam thickness, and which should be used when implementing an adjusted thickness method?). Recall that smaller-displacement cases tended to contain voussoir arching within individual layers, and that midspan crushing controls inelastic beam deformation. Therefore, the analysis minimized the difference between the model midspan and analytical stresses using $E_{rmx}$, as the majority of models had developed largely independent voussoir arches in each layer of the composite beam. Subsequent statistical analysis of the relationship between model inputs and back calculated effective thickness identified that the individual beam thickness, $E_{rmx}$, and number of layers were critical controls on the effective thickness required to most accurately account for model maximum midspan stresses using the analytical

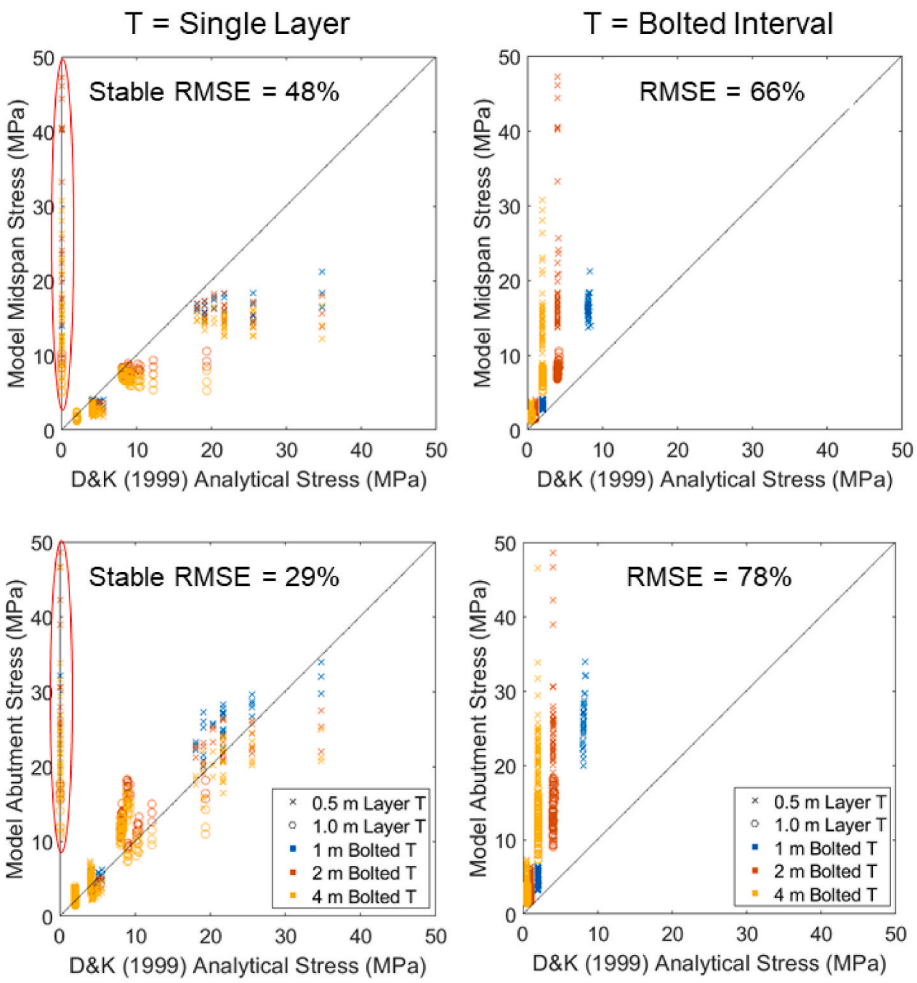


**Fig. 11.** Comparison of the Diederichs & Kaiser[3] analytical stress solution and model midspan (top) and abutment (bottom) horizontal stress results when considering the thickness input to be a single layer (left), or the entire bolted beam interval (right). Note that results that plot on the y-axis (i.e. x = 0, circled in red) indicate that the analytical solution predicted an unstable result, but model results indicated stability had been maintained. A 1:1 trend line is shown in black and a percent RMSE has been calculated for the results where both model and the analytical solution predicted stability. (For interpretation of the references to colour in this figure legend, the reader is referred to the Web version of this article.)

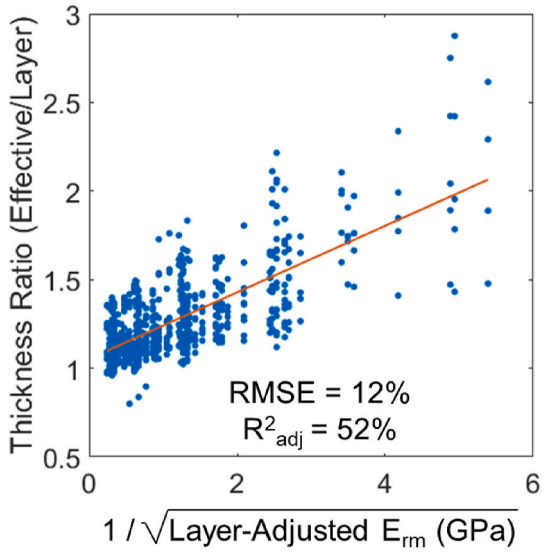


**Fig. 12.** Two-dimensional non-linear regression of effective thickness ratio results and layer-adjusted Erm calculated using Eqn. (4).

solution. When calculating the effective thickness ratio for use in the baseline Diederichs & Kaiser[3] analytical solution, $E_{rmx}$ and number of layers were considered simultaneously through the previously developed layer-adjusted $E_{rm}$ ($E_{rmn}$) (Fig. 12).

This resulted in a 12% RMSE, an R2-adjusted of 52% and the following best-fit equation:

$$\frac{T_e}{T_i} = 0.19^* \frac{1}{\sqrt{E_{rmn}}} + 1.05 \quad (5)$$

where $T_e$ = effective thickness, $T_i$ = individual layer thickness, and $E_{rmn}$ = layer-adjusted rockmass modulus in GPa (Eqn. (4)). As the number of layers in the bolted beams decreases, or as the material stiffness, joint stiffness, and joint spacing increase (i.e. $E_{rmn}$ increases), the effective thickness ratio approaches 1.05. The $T_e$ values derived from Eqn. (5) were then utilized in the baseline Diederichs & Kaiser[3] analytical solution (i.e. using $E_{rmx}$) to evaluate the accuracy of the effective thickness method in predicting model midspan stresses (Fig. 13).

This method provided much higher accuracy than either method that directly utilized the baseline Diederichs & Kaiser[3] solution, as shown in Fig. 11. The percent RMSE decreased by half and only 16 of the 69 misclassified models were still misclassified. The remaining error was restricted to models featuring 2 or 4 m bolted thicknesses and thin individual layers (i.e. 0.5 m thick). This was related to the combined influence of bolt spacing and bolted thickness, discontinuous beam deformation, and inverted stresses (i.e. abutment stresses lower than midspan). As in the case of the stiffness adjustment for beam displacement prediction, additional non-linear regressions considering individual model inputs and various combinations were undertaken to assess the point for model improvement (Table 5).

Regressions 2a-c and 3 resulted in effective thickness equations that were tested in the Diederichs & Kaiser[3] analytical solution with no significant changes in predictive accuracy. Although the added

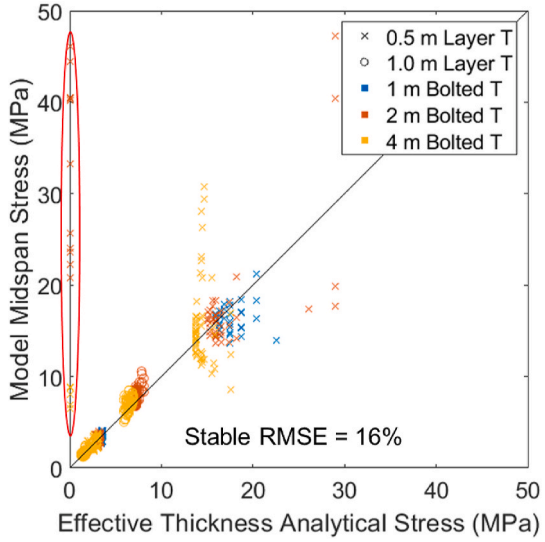


**Fig. 13.** Comparison of the effective thickness method with and stable bolted model midspan stress results. Note that the effective thickness is used in conjunction with the baseline (i.e. single-layer) $E_{rmx}$. Note that results that plot on the y-axis (i.e. x = 0, circled in red) indicate that the effective thickness analytical solution predicted an unstable result, but model results indicated stability had been maintained. A 1:1 trend line is shown in black and the percent root mean square error for results where both model and the analytical solution predicted stability. (For interpretation of the references to colour in this figure legend, the reader is referred to the Web version of this article.)

complexity in both Regression 2a-c and 3 was more accurate in estimating the "correct" effective thickness, the stresses calculated by those effective thicknesses were not significantly more accurate. Therefore, the original regression given as Eqn. (5) remains the method suggested for practical use for bolt spacings analyzed (i.e. 1.2–2.4 m).

## 4. Guidelines for application of the adjusted analytical method

A step-by-step guide to applying the methods presented above is provided to present how the adjusted analytical methods should be implemented in practice. Note that the limitations of these adjustments are largely the same as those of the baseline Diederichs & Kaiser[3] analytical method, which remains the more conservative method from a design standpoint. The adjusted methods should only be applied to flat-roof excavations in homogeneous, well-jointed rockmasses (i.e. RMR > 50). Furthermore, the adjusted methods developed in this study have not been verified for dipping excavations, and the impact of bolt spacing has only been explicitly considered for the spacings tested herein.

### 4.1. Maximum displacement determination

In order to determine maximum midspan displacement, the required analytical inputs include beam span, bolted thickness, layer thickness, specific weight, Young's Modulus, joint normal stiffness, and horizontal (i.e. bedding) joint spacing. Account for anticipated surcharge pressure (i.e. groundwater or weak back) or support pressure from suspension elements (i.e. cable bolts) by adjusting the beam specific weight using the appropriate formulae from Diederichs & Kaiser.[3] The only adjustments to the baseline Diederichs & Kaiser[3] analytical solution required are to the beam thickness and the rockmass modulus.

The beam thickness should be set equal to the bolted interval and the rockmass modulus in the horizontal direction should be calculated as:

$$\frac{1}{E_{rmx}} = \frac{1}{E} + \frac{1}{(jkn)s_j} \tag{6}$$

**Table 5**
Coefficients, p-values, and $R^2$-Adjusted for multiple linear regressions considering the effect of additional model inputs on the effective thickness. $E_{rmn}$ = Layer-adjusted $E_{rm}$.

| Bolt Spacing | Variable | Coefficient | p-value | $R^2$ Adjusted |
|---|---|---|---|---|
| | **Regression 1 – Fig. 12** | | | |
| **All** | 1/sqrt($E_{rmn}$) | 0.19 | <1.0 (10)$^{-6}$ | 0.52 |
| | Intercept | 1.06 | <1.0 (10)$^{-6}$ | |
| | Bolted Thickness | −0.001 | 0.9 | |
| | Intercept | 1.09 | <1.0 (10)$^{-6}$ | |
| | **Regression 2a-c** | | | |
| **1.2** | 1/sqrt($E_{rmn}$) | 0.26 | <1.0 (10)$^{-6}$ | 0.71 |
| | Vertical Joint Spacing | 0.09 | <1.0 (10)$^{-6}$ | |
| | Intercept | 0.93 | <1.0 (10)$^{-6}$ | |
| **1.8** | 1/sqrt($E_{rmn}$) | 0.20 | <1.0 (10)$^{-6}$ | 0.67 |
| | Vertical Joint Spacing | 0.09 | <1.0 (10)$^{-6}$ | |
| | Intercept | 0.93 | <1.0 (10)$^{-6}$ | |
| **2.4** | 1/sqrt($E_{rmn}$) | 0.11 | <1.0 (10)$^{-6}$ | 0.42 |
| | Vertical Joint Spacing | 0.11 | <1.0 (10)$^{-6}$ | |
| | Intercept | 0.95 | <1.0 (10)$^{-6}$ | |
| | **Regression 3** | | | |
| **All** | 1/sqrt($E_{rmn}$) | 0.20 | <1.0 (10)$^{-6}$ | 0.63 |
| | Bolts/m | 0.31 | <1.0 (10)$^{-6}$ | |
| | Vertical Joint Spacing | 0.10 | <1.0 (10)$^{-6}$ | |
| | Intercept | 0.74 | <1.0 (10)$^{-6}$ | |

The layer-adjusted rockmass modulus of the beam should be calculated based on the number of layers (n) in the bolted interval as:

$$E_{rmn} = Cx^{*}E_{rmx} \tag{7}$$

where:

$$Cx = \frac{1.1}{n^2} \tag{8}$$

The iterative solution loop should then be run as it is in the baseline Diederichs & Kaiser[3] analytical solution. However, the only valid outputs from this analysis will be the displacement and the buckling limit.

### 4.2. Maximum stress determination

In order to determine the maximum stress, the analytical inputs required are identical to those in the previous section. The baseline rockmass modulus (Eqn. (6)) should be utilized as the beam stiffness and the effective thickness to be used in the analytical solution is be calculated as:

$$T_e = \left(0.19 * \frac{1}{\sqrt{E_{rmn}}} + 1.05\right) * T_i \tag{9}$$

where $T_i$ = individual layer thickness and $E_{rmn}$=layer-adjusted rockmass modulus in GPa.

The iterative solution loop shall then be run as it is in the baseline Diederichs & Kaiser[3] analytical solution and the maximum stress ($\sigma_{max}$) utilized to calculate the $FoS_{crushing}$ as:

$$FoS_{crushing} = \frac{UCS^*}{\sigma_{max}} * B \quad (10)$$

where UCS* = field scale unconfined compressive strength (e.g. in the absence of other information, adjusted from lab scale to field scale values with a 0.3–0.5 multiplier), and B = 0.6–1.25 multiplier depending on the post-peak behavior of the material (i.e. elastic-brittle-plastic = 0.6, perfectly plastic = 1.25).

## 5. Conclusions

Systematic analysis of voussoir beam mechanical behavior under a wide range of loading conditions has verified that simple alterations to the existing voussoir analytical solution can capture the behavior of relatively complex voussoir beam scenarios as determined using numerical models. Accounting for inelastic material behavior, as well as horizontal joints in multi-layer systems and the presence of passive rock bolts allows for practical use of the voussoir beam analog in more realistic scenarios.

This study has demonstrated that the accuracy of $FoS_{crushing}$ relies heavily on the post-peak behavior of the modeled material. Furthermore, inelastic beams did not fail unless the midspan yielded. The results suggest that an additional 0.6- or 1.25-times adjustment be made to Eqn. (3) for brittle and perfectly plastic post-peak behavior end-members, respectively, once the UCS has been adjusted to field scale values (e.g. using a multiplier 0.3–0.5 suggested in Diederichs & Kaiser[3]). This adjustment also accounts for the midspan-abutment stress discrepancy, and the propensity for brittle material to yield in tension.

A parametric sensitivity analysis of 810 models analyzed the impact of different beam sizes, joint spacings, layer thicknesses, material properties, joint properties, and bolt spacing. Stable model results were analyzed statistically to determine an effective $E_{rm}$ that minimized the difference between the displacement results of numerical and analytical methods. This adjustment value was determined to be influenced by the number of horizontal layers in a given model. The layer-adjusted $E_{rm}$ (i.e. $E_{rmn}$) was then used to predict the deflection of the bolted interval with greater accuracy than the baseline Diederichs & Kaiser[3] analytical solution. In order to predict model stresses, an analysis of effective beam thickness was conducted. The effective thickness method for midspan stress prediction also proved more accurate than the baseline Diederichs & Kaiser[3] analytical solution.

Given the mechanical complexity of the bolted voussoir models presented herein, a mathematically derived analytical solution to predict the maximum displacement and stress may not be achievable. However, the rockmass-bolt interaction has been shown to have a distinct and repeatable impact on model displacement and maximum stress. In particular, the use of either the overall beam thickness or single layer thickness in the existing Diederichs & Kaiser[3] analytical solution was shown to be either too conservative or too optimistic when applied to more complex conditions. Finally, a mechanical basis for softening of a bedded and jointed roof for use in the voussoir beam analog has been developed.

Due to the combination of predominantly bolt element shear and bolt interface normal loading towards the beam abutments, as well as the non-negligible impact of bolt element axial and bolt interface shear loading at the beam midspan, the effective stiffness and thickness of the supported voussoir beam in its simplest possible geometry (i.e. orthogonal, fully-persistent discontinuities tested herein) decrease and increase, respectively. These changes can be accounted for through the equations developed through the statistical analysis of model results to improve the accuracy of the analytical solution.

## Declaration of competing interest

The authors declare the following financial interests/personal relationships which may be considered as potential competing interests:

## Acknowledgements

This study was sponsored by the Alpha Foundation for the Improvement of Mine Safety and Health, Inc. (ALPHA FOUNDATION). The views, opinions, and recommendations expressed herein are solely those of the authors and do not imply any endorsement by the ALPHA FOUNDATION, its Directors and staff. The authors appreciate the funding provided for this project by the ALPHA FOUNDATION. The research conducted for this study was also partially funded by the National Institute of Occupational Health and Science (NIOSH) under Grant Number 200-2016-90154. Part of the modeling effort for this study was conducted as part of the first author's course of study using educational licenses of UDEC provided by Itasca Consulting, Ltd. The authors appreciate Itasca's support in this capacity.

## References

1 Fortsakis P, Nikas K, Marinos V, Marinos P. Anisotropic behaviour of stratified rock masses in tunnelling. *Eng Geol.* 2012;141–142:74–83. https://doi.org/10.1016/j.enggeo.2012.05.001.
2 Galvin JM. *Ground Engineering - Principles and Practices for Underground Coal Mining.* Springer International Publishing; 2016. https://doi.org/10.1007/978-3-319-25005-2.
3 Diederichs MS, Kaiser PK. Stability of large excavations in laminated hard rock masses: the voussoir analogue revisited. *Int J Rock Mech Min Sci.* 1999;36(1):97–117. https://doi.org/10.1016/S0148-9062(98)00180-6.
4 Ran JQ, Passaris EKS, Mottahed P. Shear sliding failure of the jointed roof in laminated rock mass. *Rock Mech Rock Eng.* 1994;27(4):235–251. https://doi.org/10.1007/BF01020201.
5 Sofianos AI, Kapenis AP. *Effect of abutment compliance on the stability of an underground bedded roof formation. ISRM International Symposium - EUROCK 1996.* 1996:833–837.
6 Sofianos AI, Kapenis AP. Numerical evaluation of the response in bending of an underground hard rock Voussoir beam roof. *Int J Rock Mech Min Sci.* 1998;35(8):1071–1086. https://doi.org/10.1016/S0148-9062(98)00166-1.
7 Tsesarsky M. *Stability of Underground Openings in Stratified and Jointed Rock.* 2005.
8 Tsesarsky M. Deformation mechanisms and stability analysis of undermined sedimentary rocks in the shallow subsurface. *Eng Geol.* 2012;133–134:16–29. https://doi.org/10.1016/J.ENGGEO.2012.02.007.
9 Hatzor YH, Benary R. The stability of a laminated Voussoir beam: back analysis of a historic roof collapse using DDA. *Int J Rock Mech Min Sci.* 1998;35(2):165–181. https://doi.org/10.1016/S0148-9062(97)00309-4.
10 Bakun-Mazor D, Hatzor YH, Dershowitz WS. Modeling mechanical layering effects on stability of underground openings in jointed sedimentary rocks. *Int J Rock Mech Min Sci.* 2009;46(2):262–271. https://doi.org/10.1016/j.ijrmms.2008.04.001.
11 Alejano LR, Taboada J, García-Bastante F, Rodriguez P. Multi-approach back-analysis of a roof bed collapse in a mining room excavated in stratified rock. *Int J Rock Mech Min Sci.* 2008;45(6):899–913. https://doi.org/10.1016/J.IJRMMS.2007.10.001.
12 Pells P, Best RJ. Aspects of primary support design for tunnels in the Sydney Basin. *Trans Inst Eng Aust Civ Eng.* 1991;CE33(2):57–66. https://doi.org/10.1016/0148-9062(92)90957-2.
13 Shabanimashcool M, Li CC. Analytical approaches for studying the stability of laminated roof strata. *Int J Rock Mech Min Sci.* 2015;79:99–108. https://doi.org/10.1016/j.ijrmms.2015.06.007.
14 Oliveira D, Pells P. Revisiting the applicability of voussoir beam theory for tunnel design in Sydney. *Artic Aust Geomech J. Published online*; 2014. https://www.researchgate.net/publication/289162654. Accessed October 12, 2020.
15 Oliveira D, Paramaguru L. Laminated rock beam design for tunnel support. *Aust Geomech J.* 2016;51(3):1–17.
16 Please CP, Mason DP, Khalique CM, et al. Fracturing of an Euler-Bernoulli beam in coal mine pillar extraction. *Int J Rock Mech Min Sci.* 2013;64:132–138. https://doi.org/10.1016/j.ijrmms.2013.08.001.
17 Hudson J, Harrison J, Popescu M. Engineering rock mechanics: an introduction to the principles. *Appl Mech Rev.* 2002;55(2):B30. https://doi.org/10.1115/1.1451165.
18 Evans WH. The strength of undermined strata. *Am Inst Min Metall Eng.* 1941;50:475–500.
19 Fayol H. *Note sur les mouvements de terrain provoquée par l'exploitation des mines.* 1885.
20 Jones O, Llewellyn-Davies E. Pillar and stall working under a sandstone roof. *Am Inst Min Eng.* 1929;76:313–329.
21 Bucky PB, Taborelli RV. Effects of immediate roof thickness in longwall mining as determined by barodynamic experiments. *Am Inst Min Metall Eng.* 1938;96.
22 Sterling RL. *The ultimate load behavior of laterally constrained rock beams. The 21st U.S. Symposium on Rock Mechanics (USRMS).* American Rock Mechanics Association; 1980:11.
23 Beer G, Meek J. Design curves for roofs and hanging-walls in bedded rock based on "voussoir" beam and plate solutions. *Institution of Mining and Metallurgy Transactions.* 1982.

24 Sofianos AI. Analysis and design of an underground hard rock voussoir beam roof. *Int J Rock Mech Min Sci Geomech Abstr*. 1996;33(2):153–166. https://doi.org/10.1016/0148-9062(95)00052-6.

25 Yiouta-Mitra P, Sofianos AI. Multi-jointed stratified hard rock roof analysis and design. *Int J Rock Mech Min Sci*. 2018;106:96–108. https://doi.org/10.1016/j.ijrmms.2018.03.021.

26 Stimpson B, Ahmed M. Failure of a linear Voussoir arch: a laboratory and numerical study. *Can Geotech J*. 1991;29(2):188–194. https://doi.org/10.1139/t92-022.

27 Poeck EC. *Analyzing the Potential for Unstable Mine Failures with the Calculation of Released Energy in Numerical Models*. 2016.

28 Abousleiman R. *Comparitive Geomechanical Investigation of Empirical, Analytical, and Numerical MMethods Utilized in Designing Flat-Roof Excavations in Discontinuous and Laminated Rockmasses*. 2021.

29 Abousleiman R, Walton G, Sinha S. Expanding understanding of the voussoir beam analog in flat roof excavations using the discrete element method. In: *http://onepetro.org/ARMAUSRMS/proceedings-pdf/ARMA20/All-ARMA20/ARMA-2020-1205/2265229/arma-2020-1205.pdf*; 2020. Accessed July 10, 2021.

30 Tulu IB, Esterhuizen GS, Mohamed KM, Klemetti TM. *Verification of a calibrated longwall model with field measurements. 51st US Rock Mechanics/Geomechanics Symposium*; 2017. https://www.onepetro.org/download/conference-paper/ARMA-2017-0238?id=conference-paper%2FARMA-2017-0238. Accessed June 18, 2019.

31 Bahrani N, Hadjigeorgiou J. Explicit reinforcement models for fully-grouted rebar rock bolts. *J Rock Mech Geotech Eng*. 2017;9(2):267–280. https://doi.org/10.1016/j.jrmge.2016.07.006.

32 Itasca Consulting Group Inc. UDEC-universal Distinct Element Code, version 6.0. Published online 2014.

33 Salamon MDG. Elastic moduli of a stratified rock mass. *Int J Rock Mech Min Sci*. 1968;5(6):519–527. https://doi.org/10.1016/0148-9062(68)90039-9.

34 Amadei B, Goodman RE, U.S.. Formulation of complete plane strain problems for regularly jointed rocks. *22nd U.S. Symposium on Rock Mechanics, USRMS*. 1981:245–251. https://doi.org/10.1016/0148-9062(82)91201-3, 1981.

35 Huang TH, Chang CS, Yang ZY. *Elastic Moduli for Fractured Rock Mass*. 28. 1995.

36 Yoshinaka R, Yamabe T. Joint stiffness and the deformation behaviour of discontinuous rock. *Int J Rock Mech Min Sci*. 1986;23(1):19–28. https://doi.org/10.1016/0148-9062(86)91663-3.